

Interdecadal variability in an idealized model of the North Atlantic

Andrew J. Weaver

School of Earth and Ocean Sciences, University of Victoria, Victoria, British Columbia, Canada

Stella M. Aura

Department of Atmospheric and Oceanic Sciences, McGill University, Montreal, Quebec, Canada

Paul G. Myers

School of Earth and Ocean Sciences, University of Victoria, Victoria, British Columbia, Canada

Abstract. A coarse resolution model is developed to study the thermohaline circulation of the North Atlantic. This model is driven by the annual mean Hellerman and Rosenstein wind stress field, Levitus sea surface restoring temperatures, and Schmitt, Bogden, and Dorman freshwater flux fields (mixed boundary conditions) together with various parameterizations of Arctic freshwater export into the North Atlantic. The model simulations indicate the existence of self-sustained, internal variability of the thermohaline circulation with a period of about 20 years. Associated with the variability is a large variation in the deep-water formation rate in the Labrador Sea and hence the poleward heat transport in the North Atlantic. It is shown that the variability is insensitive to the freshwater flux and wind forcing used and that the timescale for this thermally driven convective/advective oscillation is set by the cooling time of the Labrador Sea. The variability is robust to various parameterizations of Arctic freshwater export but may be suppressed if there is a strong freshwater flux through the Canadian Archipelago (or equivalently, large precipitation) into the Labrador Sea. The importance of topography, although poorly resolved in this coarse resolution study, is addressed and the results are compared with a coupled atmosphere-ocean simulation and observations taken over the North Atlantic.

1. Introduction

It has become apparent from long time series of climate/climate proxy data, which have been analyzed in recent years, that the air-sea-ice climate system exhibits substantial variability on the decadal to interdecadal timescale. For example, global surface air temperatures [Ghil and Vautard, 1991], sea surface temperature (SST) anomalies [Loder and Garrett, 1978; Kushnir, 1994], West African rainfall and the landfall of intense hurricanes on the U.S. coast [Gray, 1990], properties of North Atlantic Deep Water (NADW) formation [Lazier, 1980; Roemmich and Wunsch, 1984; Dickson *et al.*, 1988; Schlosser *et al.*, 1991], temperature and salinity characteristics and circulation of the North Atlantic [Levitus, 1989a, b, c, 1990; Greatbatch *et al.*, 1991], Arctic sea ice extent [Mysak and Manak, 1989; Mysak *et al.*, 1990], runoff from Eurasia [Cattle, 1985; Ikeda, 1990], and global sea level pressure [Krishnamurti *et al.*, 1986] all exhibit signals of decadal/interdecadal timescale. While many of these studies have been restricted to relatively short time series, the Greenland ice core data of Hibler and Johnsen [1979], show a 20-year oscillation in the North Atlantic using oxygen isotope records spanning the years 1244–1971.

The long timescale associated with this variability has led researchers to postulate that its source lies within the ocean,

in particular, the thermohaline circulation. Indeed, this hypothesis was originally put forward by Bjerknes [1964] in his attempt to explain decadal/interdecadal changes in long timeseries of SST in the subpolar North Atlantic [see also Bryan and Stouffer [1991]].

Numerical ocean general circulation model (OGCM) simulations in idealized basins have indicated the possibility of natural, internal variability of the thermohaline circulation under mixed boundary conditions [e.g., Weaver and Sarachik, 1991a, b; Winton and Sarachik, 1993] (also see Weaver and Hughes [1992] for a review). These boundary conditions reflect the fundamental difference in coupling of SST and sea surface salinity (SSS) between the ocean and the atmosphere. Under mixed boundary conditions the SST of the ocean model is restored to some apparent atmospheric temperature (or more commonly, a prescribed SST field) following the formulation of Haney [1971]. This boundary condition implies a specified timescale for the removal of SST anomalies and allows for the heat uptake/loss of the ocean to be dependent upon the ocean surface temperature. For salinity, where a specified timescale for the removal of SSS anomalies does not exist, it is more appropriate to specify a fixed salinity or freshwater flux, independent of the SSS. While these boundary conditions are admittedly crude, they do reflect the different nature of the observed SSS and SST coupling between the ocean and the atmosphere (see also Zhang *et al.* [1993]).

Associated with the decadal/interdecadal thermohaline

Copyright 1994 by the American Geophysical Union.

Paper number 94JC00521.
0148-0227/94/94JC-00521\$05.00

variability found in the coarse resolution simulations of *Weaver and Sarachik* [1991a, b] were large changes in the poleward heat transport. The changes in heat transport corresponded directly to changes in the heat lost/gained to the overlying atmosphere at high latitudes, as the ocean stored little heat during the oscillation. *Weaver et al.* [1991] concluded that the existence of decadal/interdecadal variability was linked to the existence of a large area of negative precipitation-evaporation (PE) at middle to high latitudes, together with freshwater gain further north. The meridional gradients in the freshwater flux-forcing field also had to be sufficiently strong so that the system was in a "haline dominant" regime. *Weaver et al.* [1991] suggested that when the thermohaline circulation was weak, it slowly passed through the region with negative PE, and hence the surface waters become more saline. A warm, saline surface anomaly then developed through convection and this anomaly was advected to the eastern boundary by the mean flow where it was convected to the deeper ocean (as in *Weaver and Sarachik* [1991b]), leading to the subsequent generation of a reverse cell which in turn caused the thermohaline circulation to intensify. The intensified thermohaline circulation passed rapidly through the evaporative region, and hence the surface waters did not become as saline. Deep water then formed at high latitudes until high-latitude freshening dominated and the thermohaline circulation slowed down. This whole process repeated itself with the advective timescale of the oscillation determined by the time taken for salinity and temperature anomalies, formed in the local evaporative region, to be advected to the northern boundary.

The aforementioned studies used time-invariant surface-forcing fields (notice that the actual heat flux is time varying, while the restoring temperatures are fixed). In reality the oceanic surface forcing is not steady, as the atmosphere and ocean are continually interacting with each other on small space scales and timescales. *Weaver et al.* [1993] considered these interactions as stochastic perturbations of the background forcing fields. They showed that the decadal/interdecadal internal variability still persisted when a stochastic component was added to the freshwater flux-forcing field. They further concluded that the variability was determined by the structure and strength of the mean freshwater flux field in relation to the mean thermal and wind-forcing fields. Furthermore, *Myers and Weaver* [1992] showed that seasonally varying surface forcing did not substantially alter the results.

The OGCMs discussed above were largely restricted to idealized flat-bottom basins forced by zonally averaged restoring temperatures, idealized winds (with no meridional component), and PE fluxes diagnosed from equilibria obtained under restoring boundary conditions. A natural question which arises is as follows: Does this variability carry over to more realistic general circulation models (GCMs) which incorporate irregular coastlines, topography, and more realistic surface-forcing fields? The purpose of this paper is to present some simulations of the North Atlantic thermohaline circulation driven by annual mean [*Levitus*, 1982] restoring temperatures, the annual mean [*Schmitt et al.*, 1989] North Atlantic freshwater flux field, and the annual mean [*Hellerman and Rosenstein*, 1983] wind stress field.

The outline of this paper is as follows: In section 2 the model and forcing fields are briefly described. The results from several experiments conducted in an idealized coarse

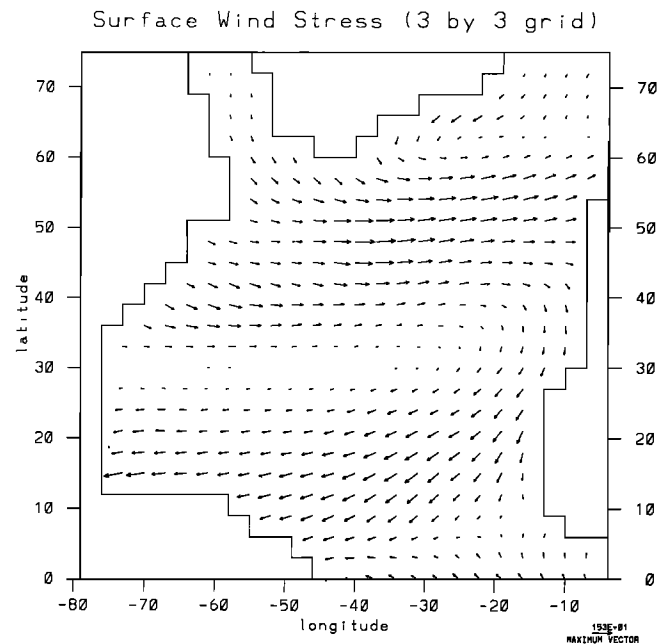


Figure 1a. *Hellerman and Rosenstein's* [1983] annual mean surface stress in dynes per square centimeter. The maximum vector shown corresponds to 1.5 dyn cm^{-2} .

resolution North Atlantic basin are then discussed in section 3. Finally, a summary and comparison with *Kushnir's* [1994] SST data and *Delworth et al.'s* [1993] coupled ocean-atmosphere model results are presented in section 4.

2. Description of the Numerical Model

In this study we employ *Cox's* [1984] version of the Bryan-Cox OGCM with $3^\circ \times 3^\circ$ horizontal resolution and 20 vertical levels ranging in thickness from 50 m at the surface to 300 m at the bottom of the basin. The basin is assumed to be flat bottomed with a depth of 4020 m except in experiments T1-T3 where bottom topography is incorporated into the model.

The surface wind stress forcing used is *Hellerman and Rosenstein's* [1983] annual mean North Atlantic data (Figure 1a), while the boundary condition employed on the model SST is a restoring condition to *Levitus's* [1982] annual mean climatology with a 50-day timescale (Figure 1b). We used *Schmitt et al.'s* [1989] annual mean freshwater flux field [Figure 1c] converted to a salt flux field (in grams of salt per square meter per second) according to the formula:

$$Q_s = \frac{\rho_0 S_0 \times \text{PE}}{\text{syr}}, \quad (1)$$

where *syr* is the number of seconds in a year, PE is the freshwater flux with units of meters per year, and S_0 is a constant reference salinity taken to be equal to the basin average salinity (35.12 practical salinity units (psu)) of the North Atlantic Ocean as calculated from *Levitus's* [1982] data.

In order to parameterize Arctic freshwater export into the North Atlantic, we added either 0.0, 0.1, or 0.2 Sv of freshwater over the top 210 m at the northern boundary depending on the experiment. The residual between the net

evaporation from *Schmitt et al.*'s [1989] data less the freshwater flux through the northern boundary was added as an additional freshwater source throughout the top 210 m at the equatorial boundary. This was done in order to keep the basin mean salinity constant throughout all integrations.

Weaver and Sarachik [1991a, b] and *Myers and Weaver* [1992] showed that in flat-bottomed OGCM experiments the use of a split time-stepping procedure for the integration of the governing equations does not alter the low-frequency variability, provided the wind forcing is steady. Thus in order to speed up the convergence of the model, we used a 2-hour timestep when integrating the barotropic vorticity and baroclinic velocity equations, while the tracer equations were integrated with a time step of 1 day or less (depending on the experiment). In the next section we quantitatively show that the use of this weak split time-stepping procedure does not affect our results by conducting two synchronous integration experiments.

The vertical eddy viscosity and diffusivity were everywhere set to $10.0 \text{ cm}^2 \text{ s}^{-1}$ and $1.0 \text{ cm}^2 \text{ s}^{-1}$, respectively, while the horizontal eddy viscosity and diffusivity were set to $1.5 \times 10^9 \text{ cm}^2 \text{ s}^{-1}$ and $1 \times 10^7 \text{ cm}^2 \text{ s}^{-1}$, respectively, over the whole domain. Convection was parameterized implicitly as enhanced vertical diffusion according to the module of *Cox* [1984]. When the water column became statically unstable, the coefficient of vertical diffusivity was assigned a value of $10^4 \text{ cm}^2 \text{ s}^{-1}$. A list of the distinguishing characteristics of all 15 experiments is presented in Table 1.

3. Results

3.1. Discussion of the Variability

In this section, attention is focused on experiment 1 in which there was no parameterization of Arctic freshwater input into the North Atlantic (Table 1). Figure 2a shows the kinetic energy density of the model ocean throughout the

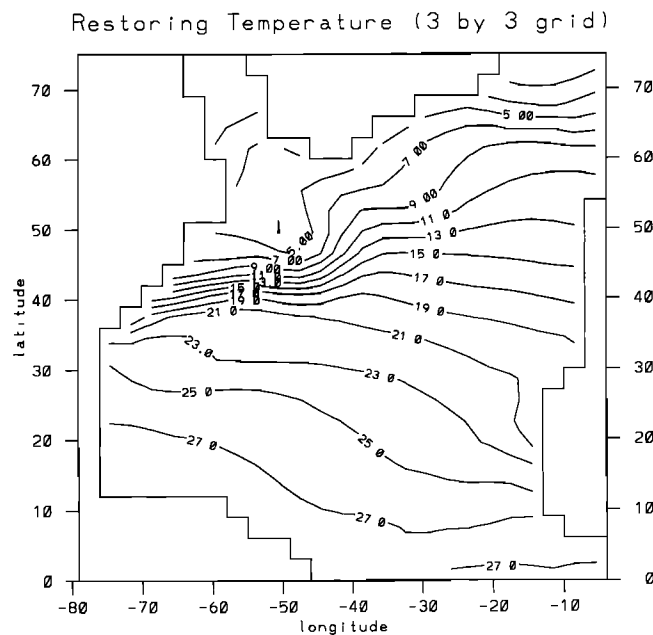


Figure 1b. *Levitus*' [1982] annual mean sea surface in degrees Celsius.

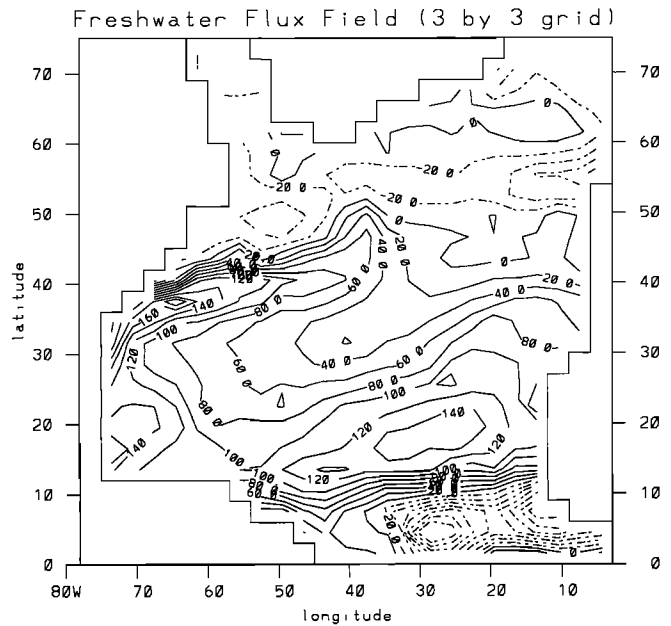


Figure 1c. Annual mean freshwater flux field of *Schmitt et al.* [1989] in centimeters per year.

3472 years of integration. What is readily evident from this time series is that the system very rapidly entered a limit cycle, the period of which is about 22 years (Figures 2b and 2c). Over the course of the oscillation the poleward heat transport varied from a maximum of about 0.8 PW at 39°N to a minimum of 0.5 PW (Figure 3). This change was associated with the shutting off and turning on of deepwater formation at the northern boundary of the Labrador Sea.

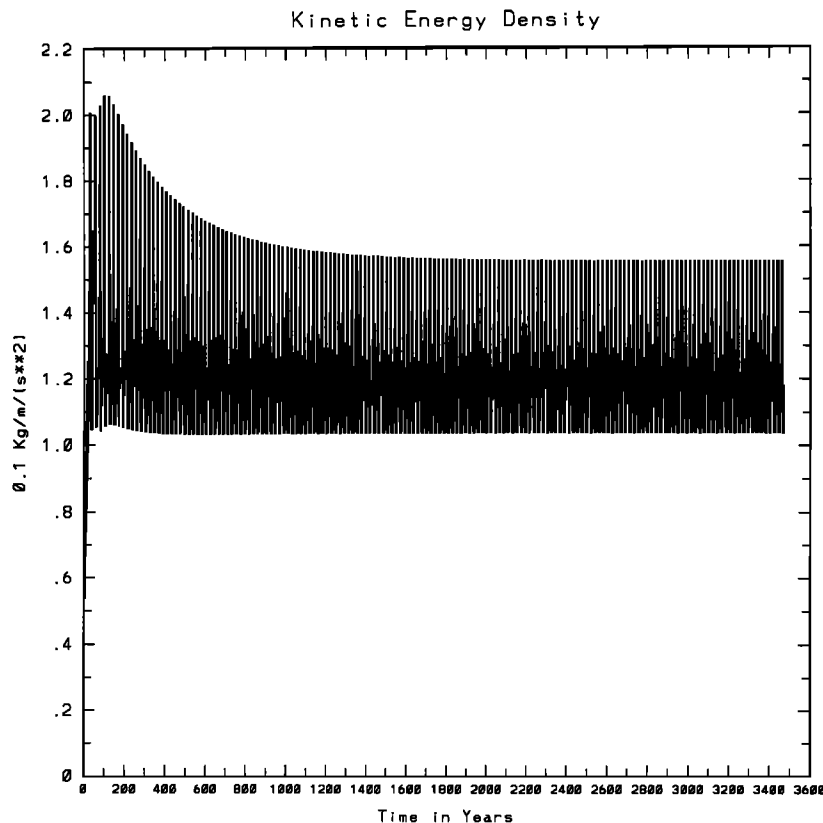
The two complete oscillations shown in Figures 2b and 2c were sampled every 2.74 years (i.e., every 1000, 1-day time steps) to produce three-dimensional fields. For the purpose of discussion we define the weak phase of the oscillation as the stage with the lowest basin mean kinetic energy and poleward heat transport (Figures 2b and 3; year 21.9). Conversely, we define the strong phase of the oscillation as the stage with the highest basin mean kinetic energy and poleward heat transport (Figures 2b and 3; year 38.3). An intermediate phase is also defined at year 32.9 in Figures 2b, 2c, and 3.

Figures 4 and 5 show the meridional overturning in the whole North Atlantic and the Labrador Sea region, respectively. Plots are shown at the weak phase (Figures 4a and 5a), intermediate phase (Figures 4b and 5b) and strong phase (Figures 4c and 5c) of the oscillation. In the weak phase (Figures 4a and 5a) about 16 Sv of deep water forms, of which about 8 Sv forms in the Labrador Sea north of 63°N . Gradients in the stream function, and hence the vertical and meridional velocity are relatively weak at this phase in the oscillation; hence the energy of the system (Figure 2b) and the poleward heat transport (Figure 3; lines 8 and 16) are at a minimum. The ocean basin is also beginning to slowly uptake the heat which it lost in the rapid phase of the oscillation (Figure 2c). As the thermohaline circulation in the Labrador Sea intensifies (Figure 5b) so does the poleward heat transport (Figure 3) until deep-water formation is suddenly triggered at the northern boundary of the Labrador Sea (Figures 4c and 5c). At this stage the thermohaline

Table 1. Characteristics of the 15 Experiments

Experiment	Arctic Flux, Sy	Location of Arctic Flux Application	Topography	Time Step Procedure	Restoring Timescale, Days	PE Forcing	Wind Forcing	Internal Variability	Period of Variability
1	0.0	n/a	flat	A	50	yes	yes	yes	22 years
S1	0.0	n/a	flat	S	50	yes	yes	yes	22 years
S2	0.0	n/a	flat	S	50	yes	yes	yes	22 years
H1	0.0	n/a	flat	A	100	yes	yes	yes	21 years
2	0.1	Labrador + GIN Seas	flat	A	50	yes	yes	no	n/a
3	0.2	Labrador + GIN Seas	flat	A	50	yes	yes	no	n/a
4	0.1	GIN Sea	flat	A	50	yes	yes	yes	17 years
5	0.1	East Greenland Current	flat	A	50	yes	yes	yes	17 years
T1	0.1	East Greenland Current	full	A	50	yes	yes	no	n/a
T2	0.1	East Greenland Current	Dredge of Labrador Sea	A	50	yes	yes	yes	17 years
T3	0.1	East Greenland Current	flat + full Labrador Sea	A	50	yes	yes	no	n/a
F1	0.0	n/a	flat	A	50	no	yes	yes	22 years
F2	0.0	n/a	flat	A	50	no	yes	yes	22 years
F3	0.0	n/a	flat	A	50	no	no	yes	22 years
F4	0.0	n/a	flat	A	50	no	no	yes	22 years

Column 1 indicates the experiment number; columns 2, 3, and 4 give the parameterized Arctic freshwater flux, where the flux was applied, and the topography used, respectively. Column 5 states whether the integration proceeded synchronously (S) or asynchronously (A); column 6 gives the restoring temperature timescale τ_R ; columns 7 and 8 indicate whether PE or wind forcing was used. The existence of any internal variability is indicated in column 9 and its period in column 10. Notice that experiments S1 and S2 are the same except for their initial conditions. Similarly, F1 and F2 and also F3 and F4 are the same except for their initial conditions.

**Figure 2a.** Kinetic energy density ($10^{-1} \text{ kg m}^{-1} \text{ s}^{-2}$) throughout the entire integration of experiment 1.

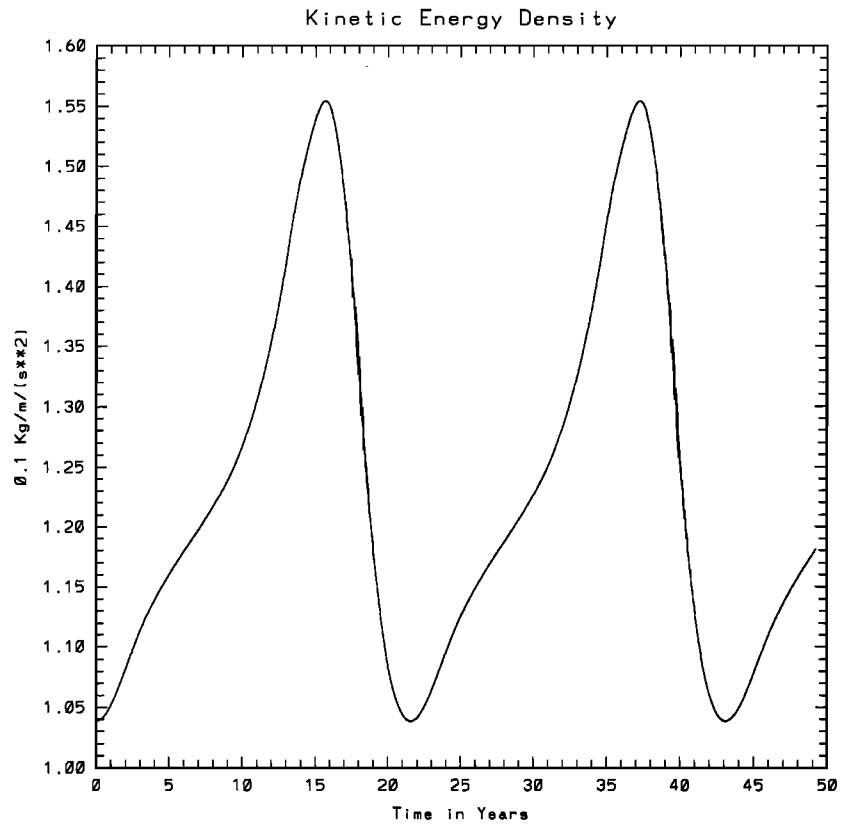


Figure 2b. Blowup of Figure 2a over the last 49 years of integration. Two complete 22-year period oscillations are resolved.

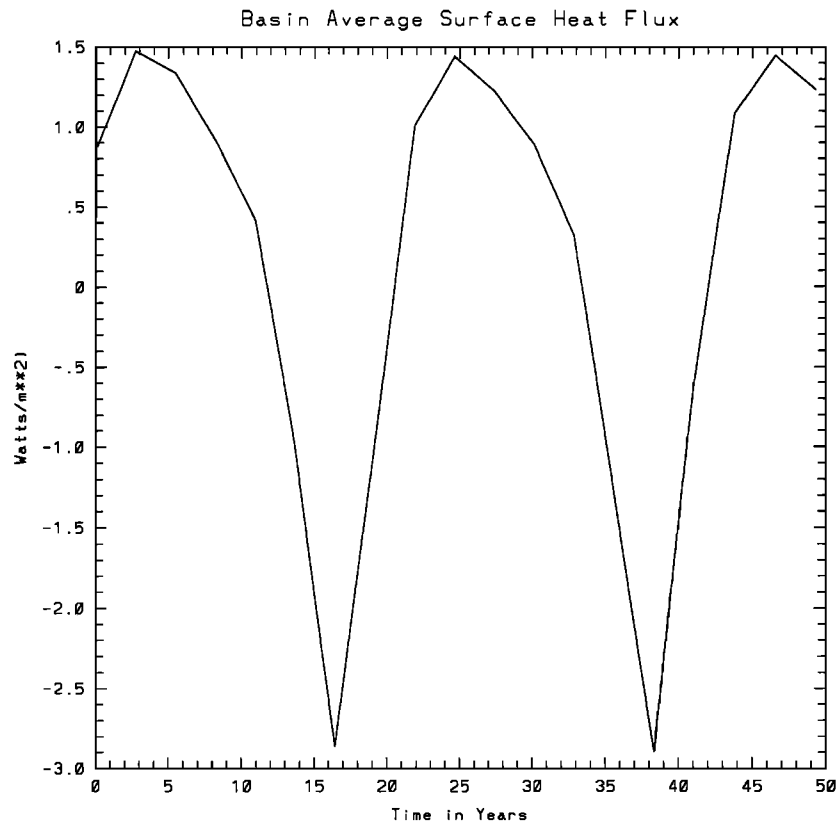


Figure 2c. Basin mean surface heat flux (in watts per square meter) during the last 49 years of integration of experiment 1. Two complete 22-year period oscillations are resolved. Positive contours indicate that the ocean is gaining heat.

Poleward Heat Transport over Oscillation

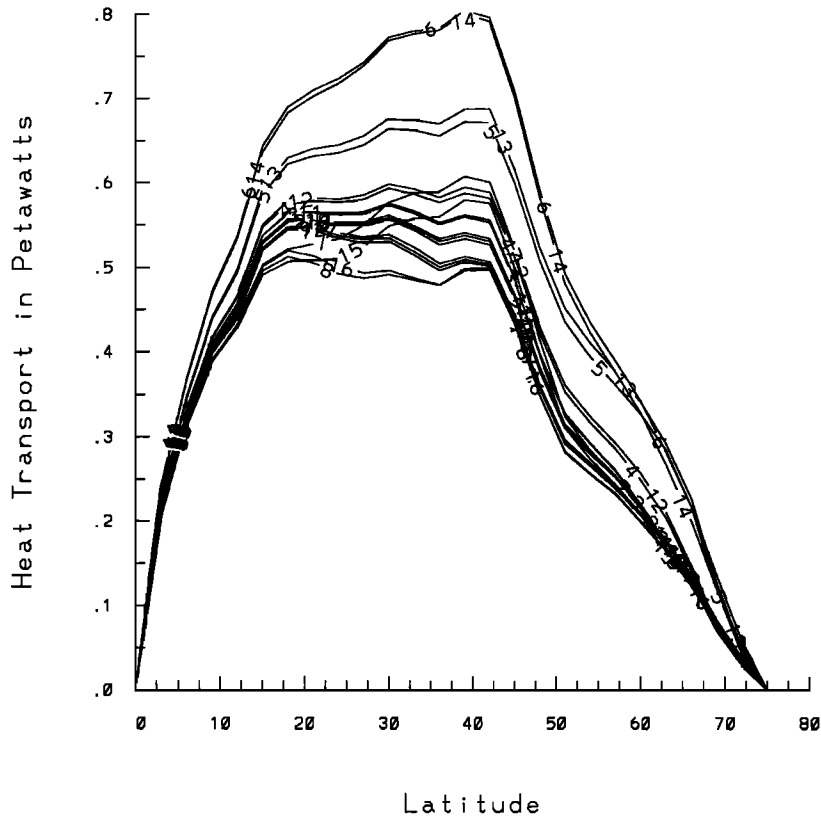


Figure 3. Poleward heat transport in petawatts ($\text{PW} \equiv 10^{15} \text{ W}$) at 2.7-year intervals throughout the 49 years shown in Figures 2b and 2c. The number n on each curve corresponds to $2.7 \times n$ years along the x axis of Figures 2b and 2c.

circulation is most intense (Figure 2b) as is its associated poleward heat transport (Figure 3; lines 6 and 14). Furthermore, the heat which the ocean had gained over the previous 13 years is rapidly lost to the overlying “atmosphere” (Figure 2c).

To test whether or not the variability was sensitive to the use of the split time-stepping procedure (asynchronous integration), two additional experiments were conducted. Experiment S1 (Table 1) started with an initial condition taken at year 3422 of experiment 1. The model was then integrated for a further 200 years with a uniform time step of 5 hours. Notice that the removal of the nonlinear terms in the momentum equations eliminated one of the most restrictive numerical stability criteria, and hence we were able to use large baroclinic velocity and barotropic vorticity equation time steps. As was to be expected, the variability was unaffected.

In experiment S2 we repeated experiment S1 but started off from a resting homogeneous ocean (with initial temperature of 5°C and salinity of 35.12 psu). The model was integrated forward for 570 years. Once more the timescale, nature, and mechanism of the variability was unchanged (Table 1).

3.2. Mechanism and Timescale of the Variability

The discussion of the physical mechanism and timescales involved in the oscillation begins from the weakest phase of the oscillation. The mechanism for the oscillation is very different from that found by *Weaver and Sarachik* [1991b] and *Weaver et al.* [1991]. As we shall see in section 3.4 the variability is insensitive to the freshwater flux or wind-forcing field used.

During the weak phase of the oscillation there is thermally driven deep convection all across the Labrador Sea (Figure 6a) and hence there is a very weak east-west pressure gradient. Consequently the meridional geostrophic flow is weak at very high latitudes in the Labrador Sea so that there is no overturning there (Figure 5a). There is still a strong north-south pressure gradient due to the surface-restoring boundary condition on temperature (Figure 7a). Associated with this north-south pressure gradient is a zonal flow (Figure 8a), which converges at the western boundary of Greenland (near 62°N), where it causes sinking and a return deep-zonal flow below (Figure 9a).

The meridional velocity field converges on the southwestern boundary of Greenland so that at this stage the main

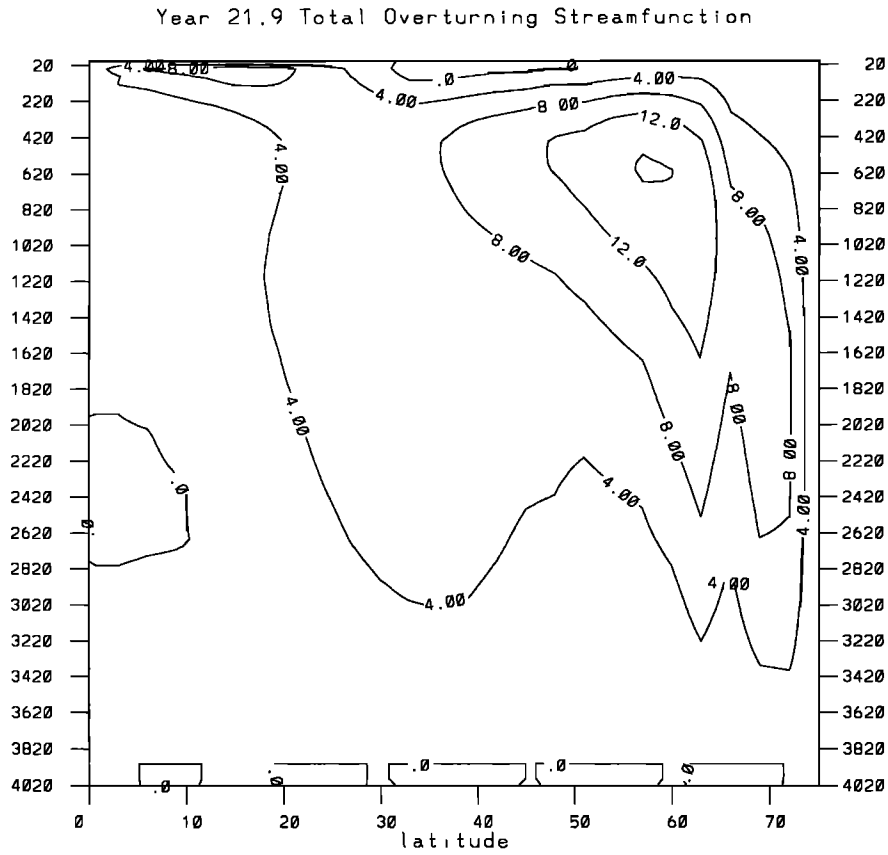


Figure 4a. Weak phase of meridional overturning streamfunction for the whole North Atlantic basin for one particular oscillation. The year in the title corresponds to the x axis of Figures 2b and 2c.

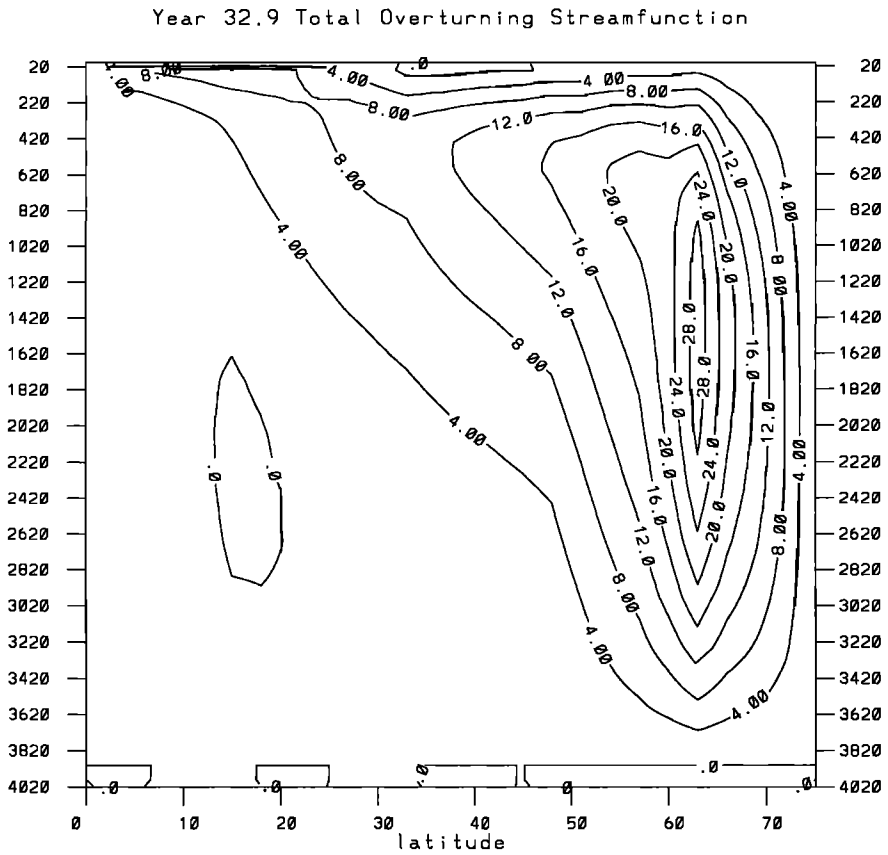


Figure 4b. Same as Figure 4a but for the intermediate phase.

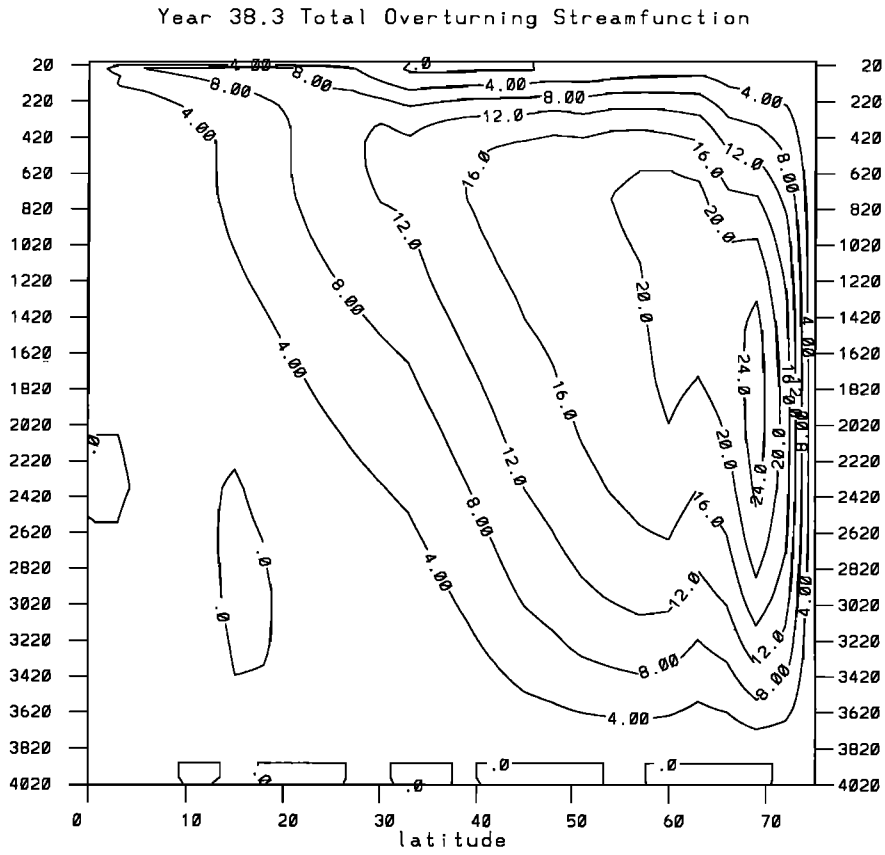


Figure 4c. Same as Figure 4a but for the strong phase.

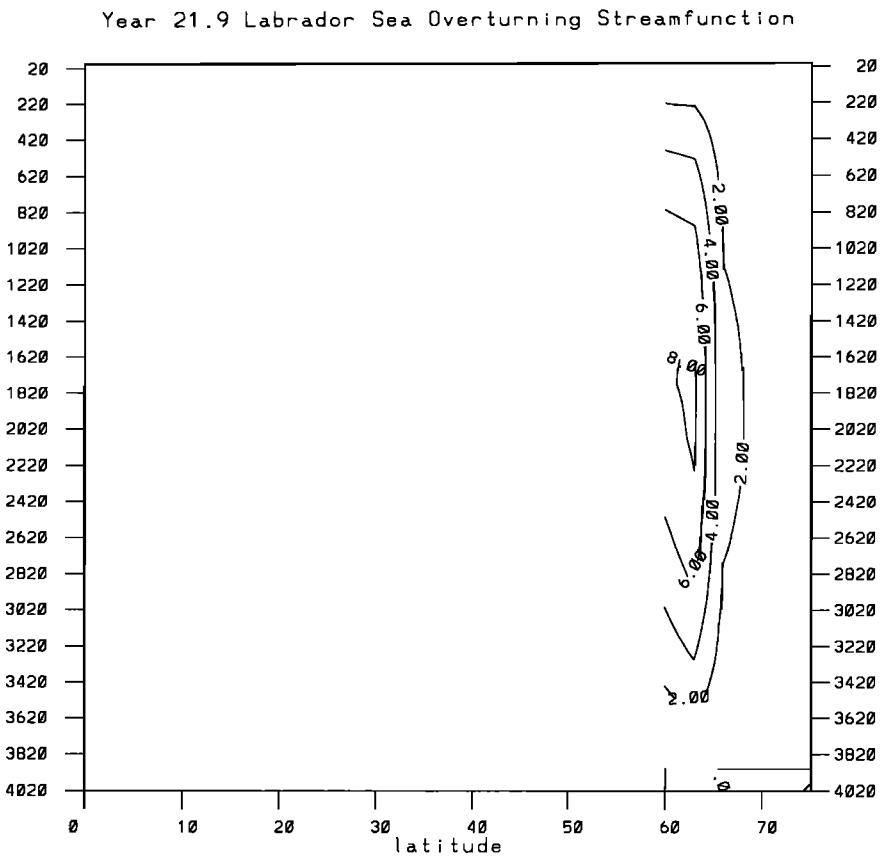


Figure 5a. Same as Figure 4a but only for the Labrador Sea region of the model domain.

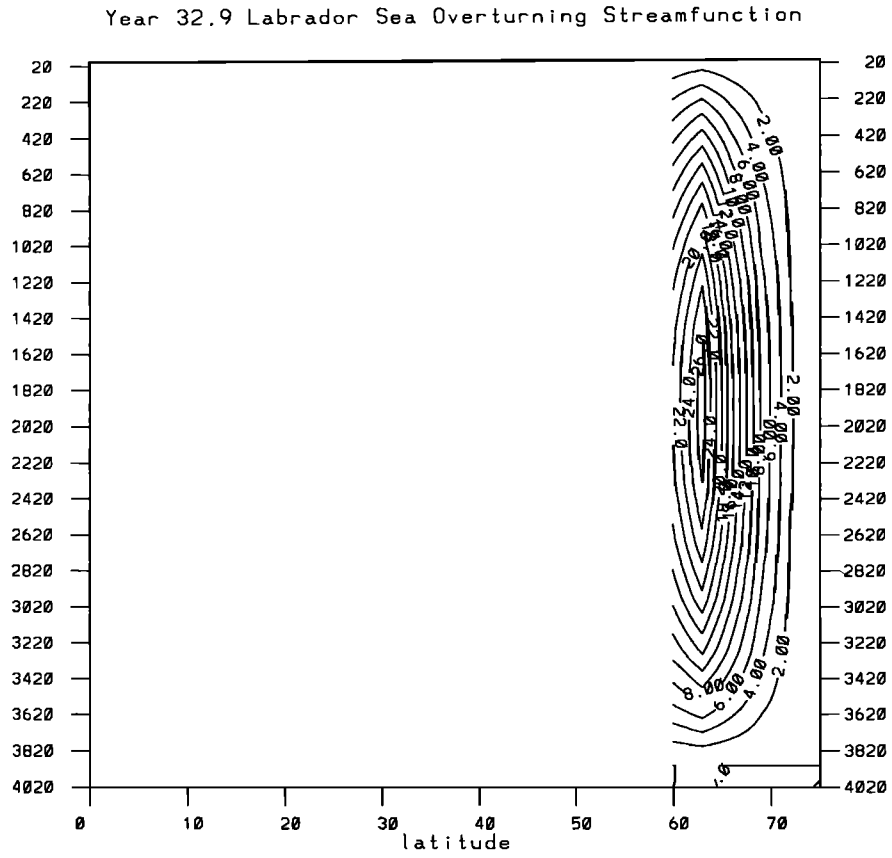


Figure 5b. Same as Figure 4b but only for the Labrador Sea region of the model domain.

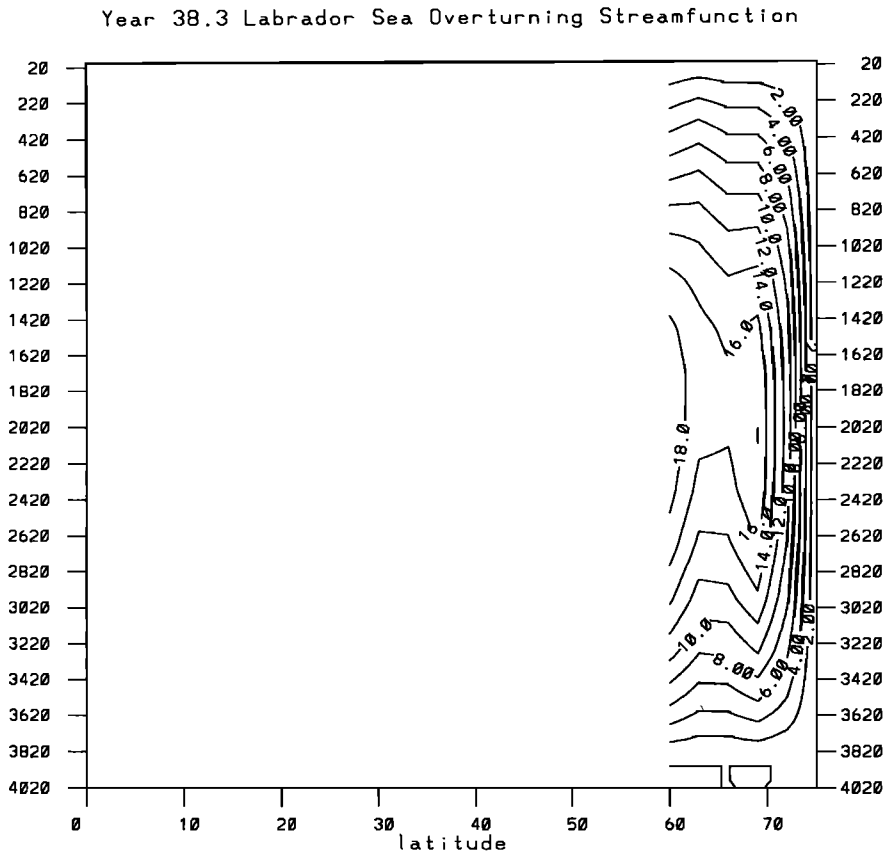


Figure 5c. Same as Figure 4c but only for the Labrador Sea region of the model domain.

Year 21.9 Temperature Cross-Section at 64.5N

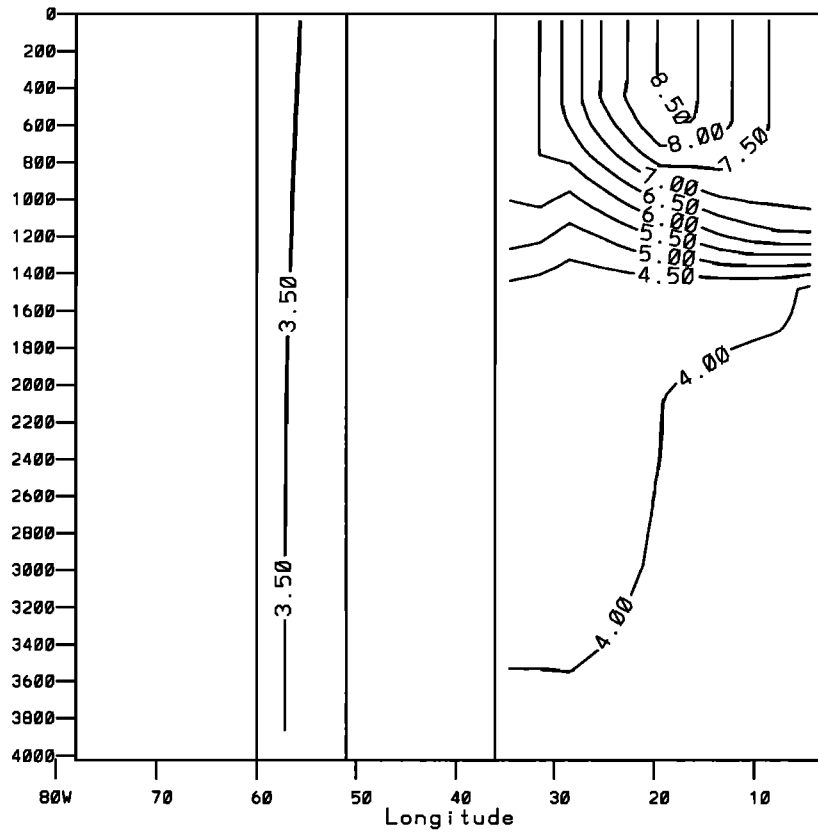


Figure 6a. Horizontal section of potential temperature at 64.5°N at the weak phase of the oscillation. The year in the title corresponds to the x axis of Figures 2b and 2c.

Year 32.9 Temperature Cross-Section at 64.5N

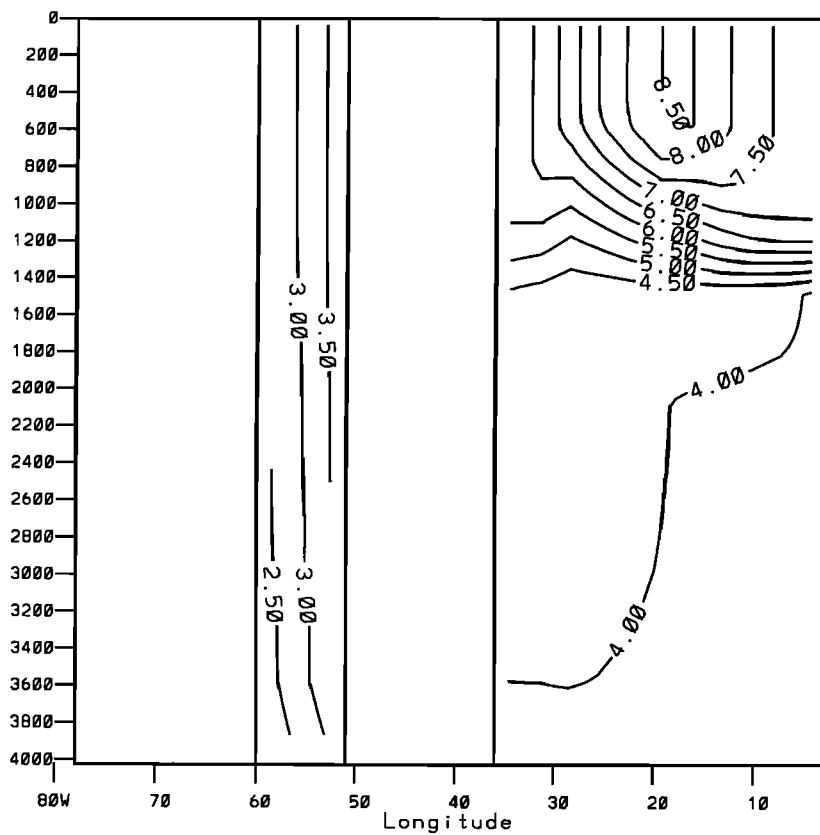


Figure 6b. Same as Figure 6a but for the intermediate phase.

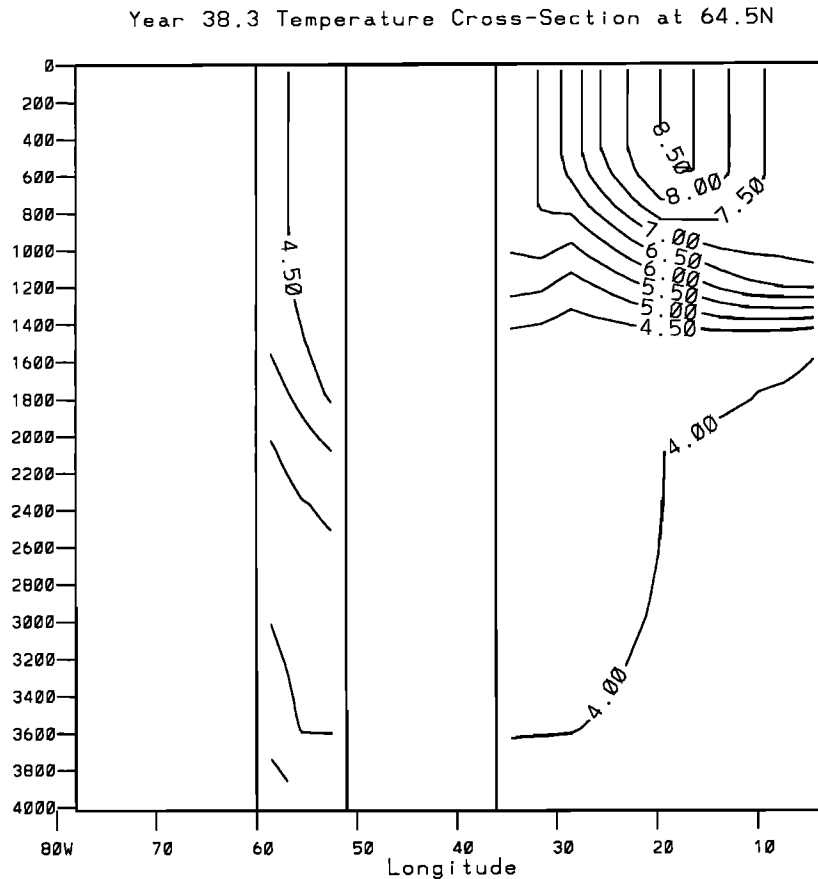


Figure 6c. Same as Figure 6a but for the strong phase.

component of Labrador Sea overturning is formed between 60° and 63°N (see Figures 5a and 9a). Notice that during the previous strong phase of the oscillation, warm, saline waters are brought into the Labrador Sea. The surface boundary conditions remove the SST anomalies faster than the SSS anomalies, and hence the net surface density gradient during the weak phase still increases as one progresses northward into the Labrador Sea, as temperature gradients dominate over salinity gradients. Since the SST and SSS are nearly zonally uniform and as convection is occurring to the bottom of the basin, there is only a very weak east-west pressure gradient in this weak phase so that deep water does not form at the northern boundary. Overturning in the “Greenland-Iceland-Norwegian Sea” (GIN Sea) now dominates the total overturning at high latitudes (Figure 4a).

The surface-restoring boundary condition on temperature takes the form (in watts per square meter; positive Q_T means heat out of the ocean):

$$Q_T = \frac{\rho_0 C_p \Delta z_1}{\tau_R} [T_1(\lambda, \phi) - T_L(\lambda, \phi)], \quad (2)$$

where $T_1(\lambda, \phi)$ is the upper ocean box (with thickness $\Delta z_1 = 50$ m) temperature at longitude λ and latitude ϕ , $T_L(\lambda, \phi)$ is the Levitus-restoring temperature (Figure 1b), C_p is the specific heat at constant pressure (~ 4000 Jkg $^{-1}$ °C $^{-1}$), ρ_0 is a reference density (~ 1000 kg m $^{-3}$), and $\tau_R = 50$ days is a restoring timescale.

During the intermediate phase of the oscillation the warm, saline waters in the high-latitude region of the Labrador Sea are being cooled toward the Levitus climatological temper-

ature. Since convection is occurring to the bottom of the basin in the Labrador Sea on a rapid timescale ($H^2/A_{TV} \approx 1/2$ year for a depth $H = 4020$ m and a vertical diffusivity $A_{TV} = 10^4$ cm 2 s $^{-1}$), condition (2) is equivalent to restoring the 4020 m deep basin to the surface value with an e -folding timescale of 11 years (assuming $T_1 - T_L$ is constant). Thus during this 11-year period the entire northern region of the Labrador Sea is being cooled from top to bottom as is evident from Figure 7b.

As the high-latitude region of the Labrador Sea is cooled the meridional surface pressure gradient increases since, as in the weak phase, temperature gradients dominate over salinity gradients. For example, Figure 7b shows that the 3°C isotherm is now at 60°N compared to about 67°N in Figure 7a. Furthermore, the outcropping latitude of the 4°C isotherm has hardly changed. This increasing meridional pressure gradient from years 21.9 to 32.9 implies an increasing zonal overturning which, through divergence (and hence upwelling) at the western boundary and convergence (and hence downwelling) at the eastern boundary, leads to an enhanced zonal pressure gradient and hence to an enhanced meridional overturning (Figures 4b and 5b). The surface and deep-velocity field at the intermediate phase (Figures 8b and 9b) further illustrate the enhanced meridional flow.

The timescale for the setup of the zonal pressure gradient is linked to the zonal overturning timescale in the Labrador Sea which, assuming a 10 cm s $^{-1}$ surface current (Figure 8b), 1 cm s $^{-1}$ deep return flow (Figure 9b), and vertical velocities of the order of 0.01 cm s $^{-1}$ (Figure 10b) is about 4 years.

Year 21.9 Meridional Temperature Section

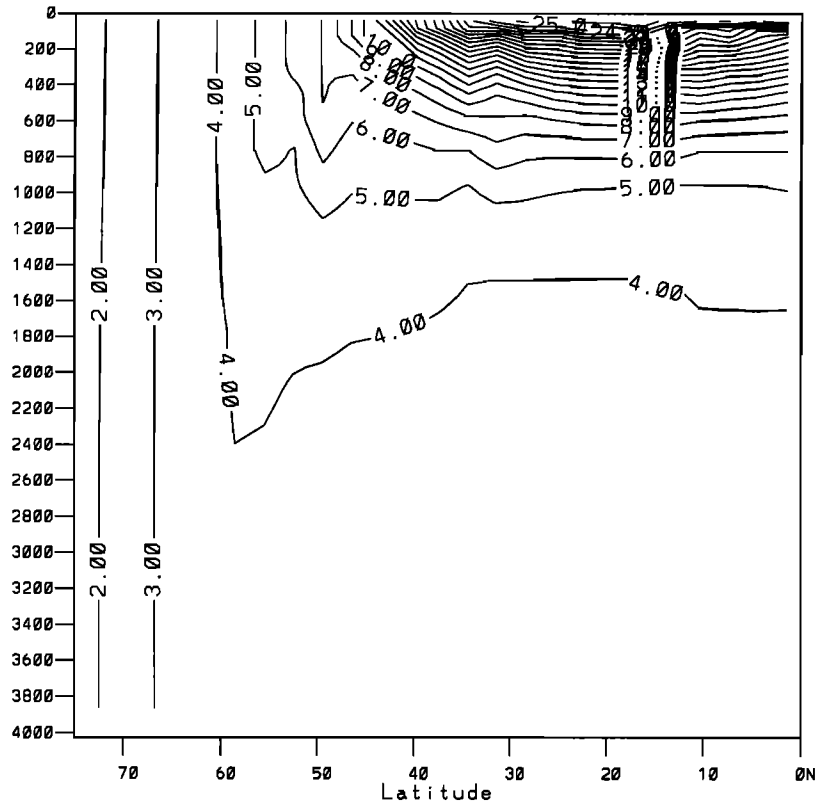


Figure 7a. Meridional section of potential temperature for the weak phase of the oscillation at the first grid point (1.5°) off the western boundary of the model domain. The year in the title corresponds to the x axis of Figures 2b and 2c.

Year 32.9 Meridional Temperature Section

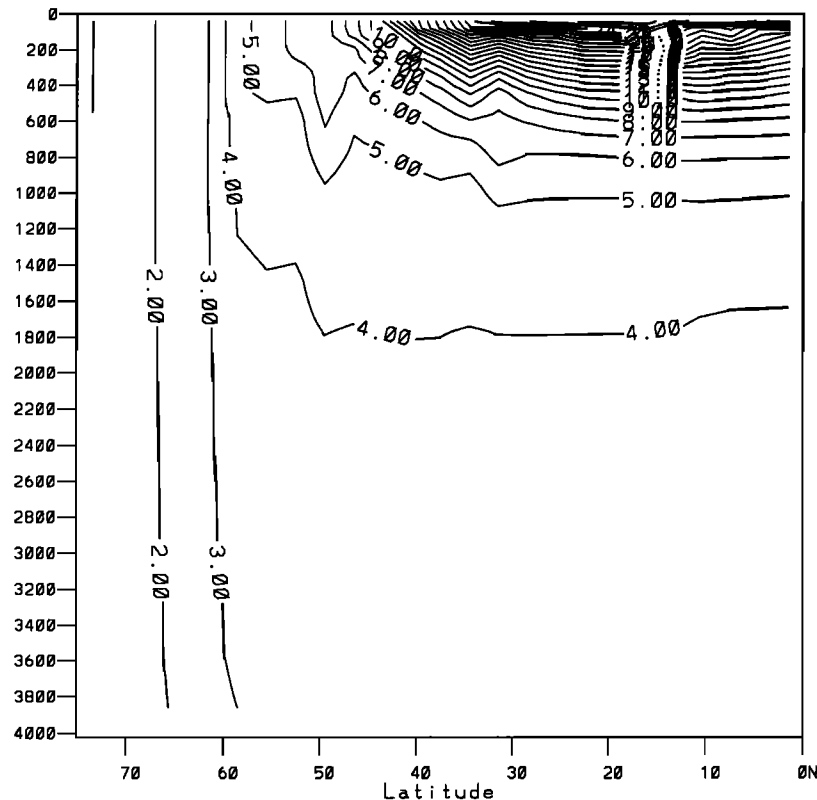


Figure 7b. Same as Figure 7a but for the intermediate phase.

Year 38.3 Meridional Temperature Section

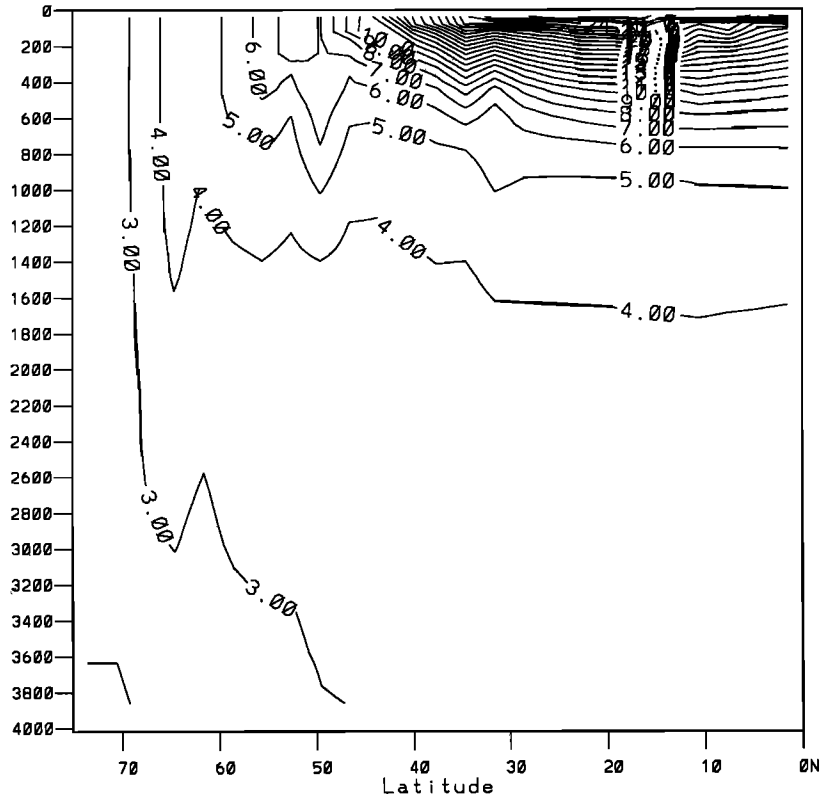


Figure 7c. Same as Figure 7a but for the strong phase.

As the meridional overturning begins to increase slightly at high latitudes, the cold and now fresh water starts to move slowly equatorward in a deep western boundary current (e.g., Figure 9b). Once this cold water has traveled a few

degrees southward it suddenly shuts off convection from below at the western boundary (e.g., Figures 6b and 6c). This follows since the cold, fresh deep water is denser than the overlying warm, saline water. The zonal pressure gradient is then further enhanced, and hence the overturning

Year 21.9 Velocity at Depth Z=25m

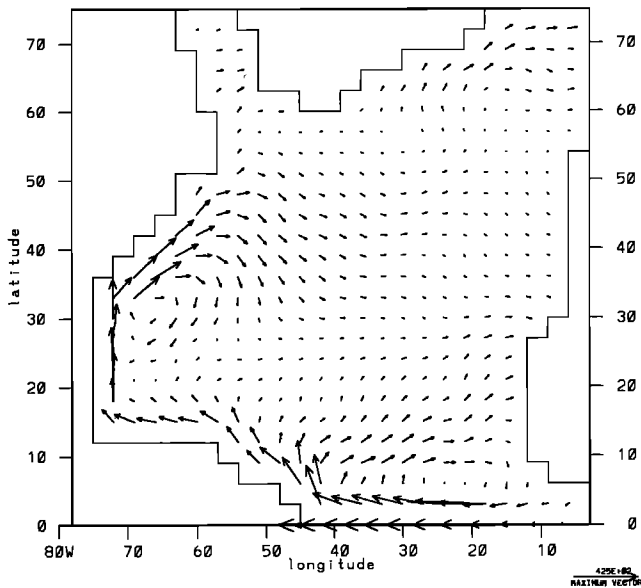


Figure 8a. Horizontal velocity at the top model level at the weak phase of the oscillation. The year in the title corresponds to the x axis of Figures 2b and 2c.

Year 32.9 Velocity at Depth Z=25m

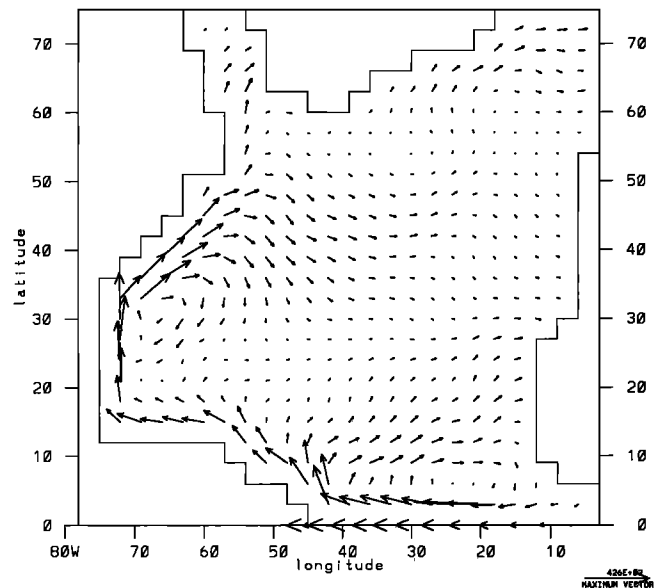


Figure 8b. Same as Figure 8a but for the intermediate phase.

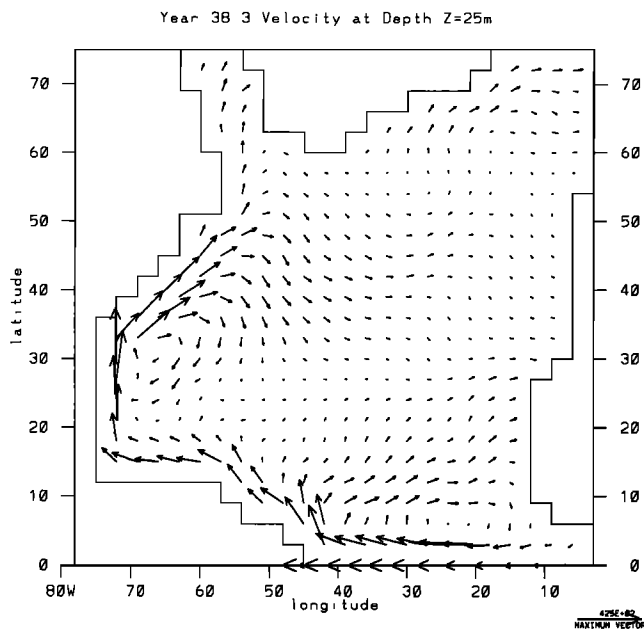


Figure 8c. Same as Figure 8a but for the strong phase.

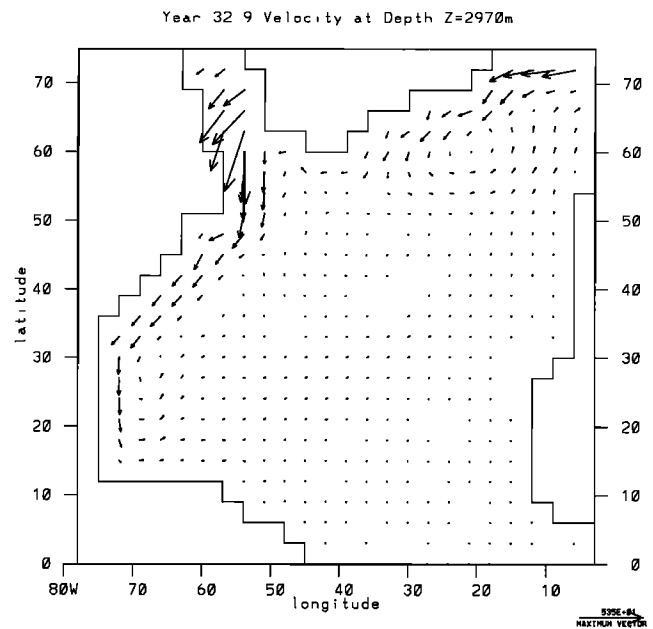


Figure 9b. Same as Figure 8b but at a depth of 2970 m.

strengthens even further. The timescale for the southward advection of this cold, fresh water is approximately 1 year, assuming an advective speed of 2 cm s^{-1} over a distance of 600 km.

Once convection is shut off in the west the overturning starts to increase rapidly and the cold, fresh high-latitude water mass is advected equatorward (in a deep western boundary current) and replaced by warm, salty water which originated in the surface waters at lower latitudes (Figure 7c). This is now the strong phase of the oscillation when the system is most energetic (Figure 2b), the heat loss is greatest (Figure 2c), and the poleward heat transport is the strongest (Figure 3; lines 6 and 14). Deep water is now forming at the

northern boundary of the Labrador Sea (Figures 5c and 10c), and the flow in the Labrador Sea is strongest and oriented meridionally.

The timescale associated with the removal of the cold, fresh high-latitude water mass and its replacement by the warm, saline mass is linked to the overturning timescale in the Labrador Sea region. Assuming a 10 cm s^{-1} surface flow (Figure 8c), a 3 cm s^{-1} deep flow (Figure 9c) over a distance of 25° (from the latitude where the western boundary current separates from the coast, 50°N (Figure 8c), to the northern boundary, 75°N), and a vertical velocity of 0.01 cm s^{-1} (Figure 10c) this timescale is about 5 years.

Since the deep basin of the Labrador Sea is now filled with

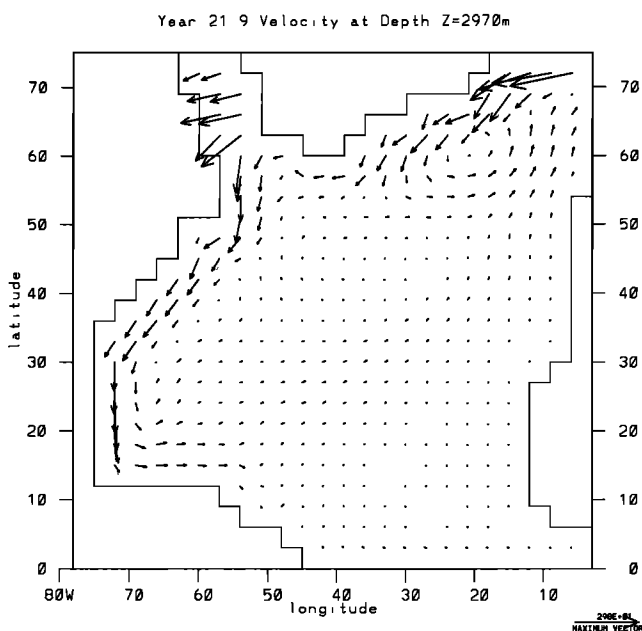


Figure 9a. Same as Figure 8a but at a depth of 2970 m.

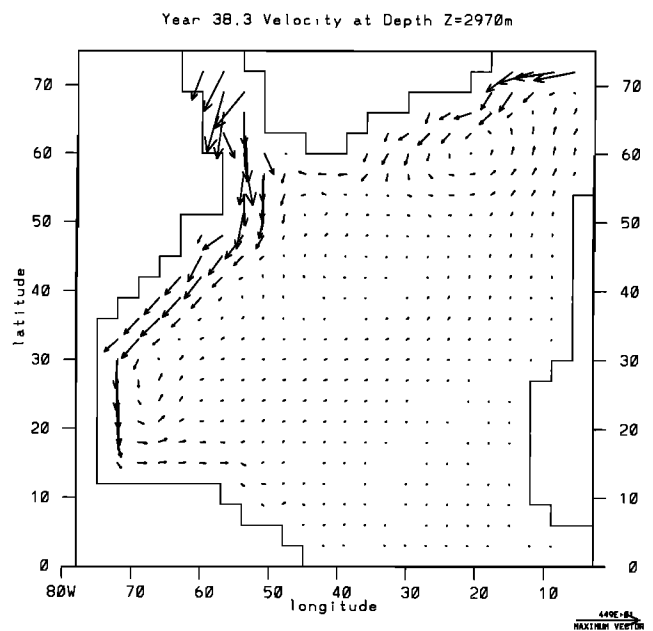


Figure 9c. Same as Figure 8c but at a depth of 2970 m.

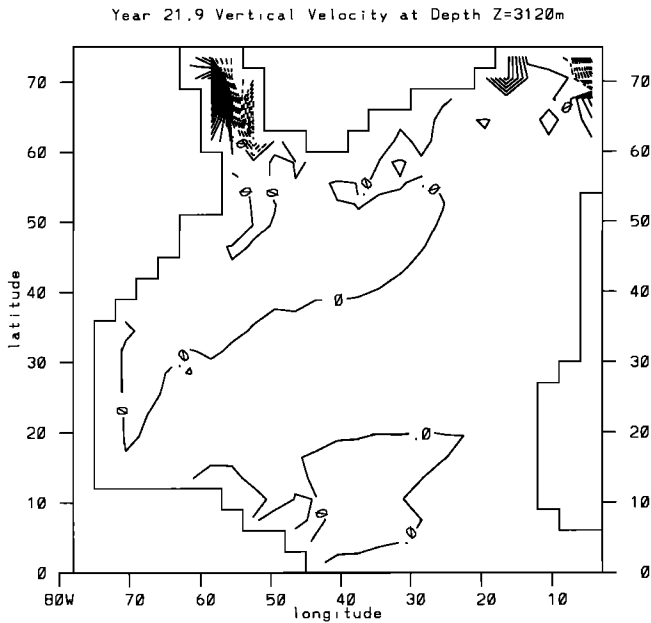


Figure 10a. Vertical velocity at a depth of 3120 m (immediately below the horizontal velocity field shown in Figure 9) at the weak phase of the oscillation. The contour interval is $2 \times 10^{-3} \text{ cm s}^{-1}$. The year in the title corresponds to the x axis of Figures 2b and 2c.

warm, saline water, convection at the surface is induced to the bottom of the basin everywhere through cooling to the Levitus SST field. Hence the zonal pressure gradient which drives the enhanced thermohaline circulation is reduced and the whole process begins again.

The total timescale of the oscillation according to the discussion above is as follows: (1) The timescale for the cooling of Labrador Sea is 11 years. (2) The timescale for

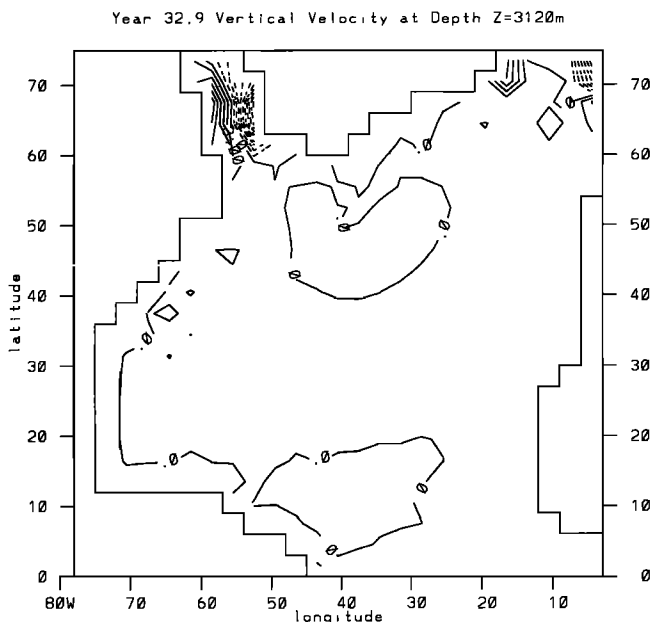


Figure 10b. Same as Figure 10a but at the intermediate phase. The contour interval is $3 \times 10^{-3} \text{ cm s}^{-1}$.

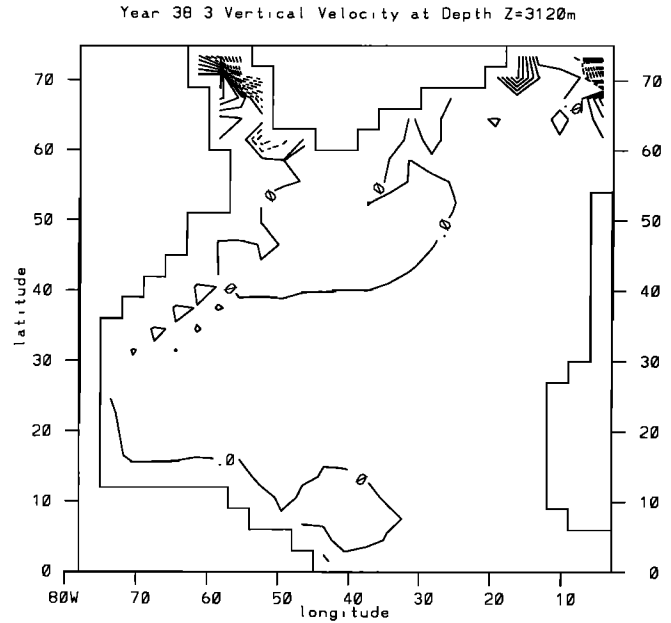


Figure 10c. Same as Figure 10a but at the strong phase. The contour interval is $2 \times 10^{-3} \text{ cm s}^{-1}$.

Labrador Sea zonal overturning and the subsequent setup of meridional pressure gradient is 4 years. (3) The timescale for the equatorward advection of cold, fresh water in the deep western boundary current is 1 year. (4) The Labrador overturning timescale for the replacement of the cold, fresh water mass by the warm, saline water mass is 5 years. Hence the approximate total timescale is 21 years. This agrees fairly well with the period of 22 years found in the model solutions.

It should be noted that the timescale for the cooling of the Labrador Sea does not scale linearly with τ_R . For example, in an additional run which was performed with $\tau_R = 100$ days instead of 50 days (experiment H1 in Table 1), the timescale of variability remained nearly the same (now 21 years). This follows, since $T_1 - T_L$ in the region of the Labrador Sea, (2), was on average about twice as large as in the $\tau_R = 50$ days integration. The result was that $(T_1 - T_L)/\tau_R$, and hence the heat flux out of the Labrador Sea, were similar in both integrations. The remainder of the mechanism was identical to that discussed above, although now deep-ocean temperatures were warmer.

The SST anomaly is shown in Figures 11a, 11b, and 11c for the weak, intermediate, and strong phase of the oscillation, respectively. From these figures it is once more clear that the variability is mainly constrained to the region of the western North Atlantic. In the weak, cooling phase of the oscillation the warm water left in the Labrador Sea from the previous rapid phase is evident (Figure 11a). Further south a $\sim 0.5^\circ$ negative temperature anomaly exists offshore, and to the west of this negative anomaly is a positive anomaly of about 0.4°C . As the Labrador Sea is cooled (Figure 11b) the thermohaline circulation intensifies, until the rapid warm phase of the oscillation occurs (Figure 11c). In this phase a $\sim 1.4^\circ\text{C}$ SST anomaly exists immediately south of the Labrador Sea.

It is relevant to point out that this SST anomaly structure and magnitude are very similar to the pattern of interdecadal SST anomaly observations shown by Kushnir [1994] as well

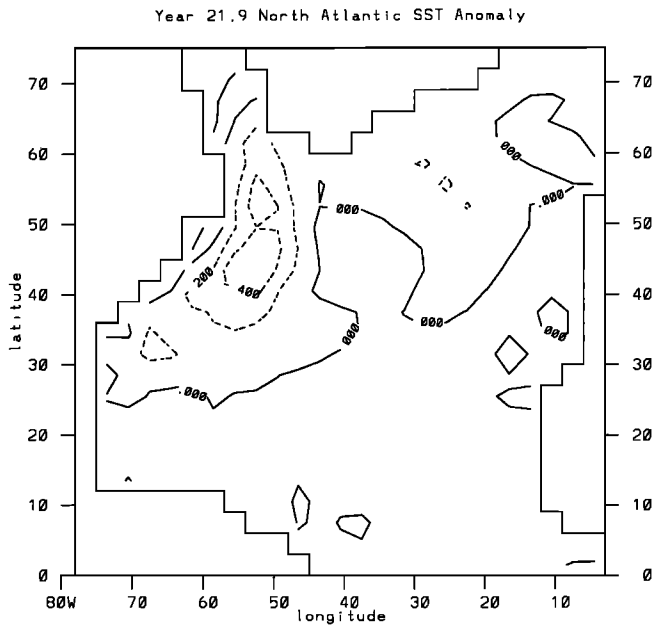


Figure 11a. Surface temperature anomaly in degrees Celsius corresponding to the weak phase of the oscillation. Dashed contours indicate negative temperature anomalies. The contour interval is 0.2°C . Notice that the anomaly is defined as a departure from the average SST over the typical oscillations shown in Figures 2b and 2c.

as the pattern of SST anomalies between the strong and weak phase of the thermohaline circulation oscillations found in the coupled ocean-atmosphere GCM simulations of *Delworth et al.* [1993]. The magnitude is slightly higher in the present calculation partially because we have examined snapshots of SST anomalies instead of long-term averages. Furthermore, we have used a relatively crude surface cou-

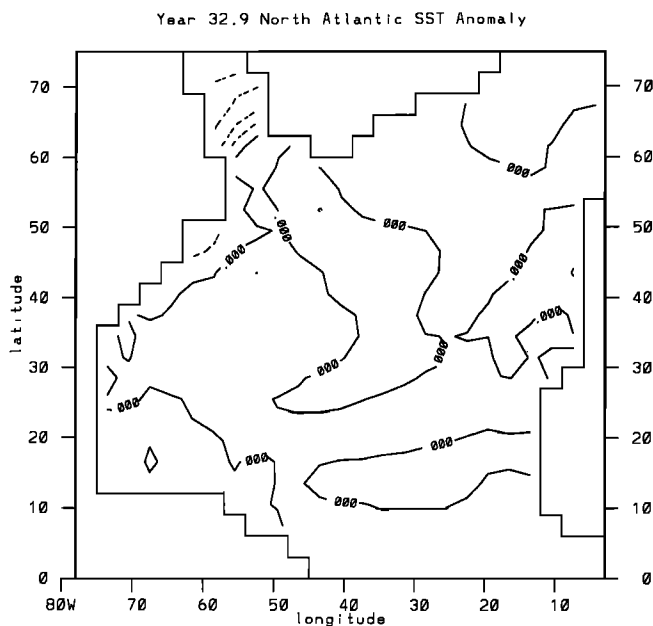


Figure 11b. Same as Figure 11a but corresponding to the intermediate phase.

pling. One might speculate that a prognostic atmosphere would dampen the variability in a fully coupled integration.

3.3. Role of Arctic Freshwater Forcing and Topography

In experiments 2–5 a flux boundary condition was applied to the top 210 m of the northern boundary in order to parameterize a transport of freshwater from the Arctic. Table 1 summarizes the location and magnitude of the flux which was applied. In the two experiments (2 and 3) in which a freshwater source was added at the northern boundary of the Labrador Sea, the internal variability discussed in the last subsection was suppressed. The external freshening was so strong that it capped convection in the Labrador Sea so the aforementioned mechanism for the variability could not occur. One can view this Arctic freshwater flux into the Labrador Sea as either a crude parameterization of flux through the Canadian Archipelago or a strong perturbation to the precipitation field. Both phenomena have the effects of capping convection and inducing a weak halocline catastrophe. In reality, a freshwater flux entering the Labrador Sea via Hudson or Davis Straits would tend to be confined to the coast in boundary currents. Only the leakage of these boundary current waters into the central Labrador Sea would affect convection.

If instead of applying 0.1 Sv all along the northern boundary it was applied only in the “GIN Sea” region (experiment 4) or only to the two grid boxes (6°) next to the Greenland coast in the eastern North Atlantic (experiment 5), the variability still occurred although now on a slightly shorter 17-year timescale. The shorter timescale was associated with a more rapid overturning timescale (points 3 and 4 in the last section) in the Labrador Sea which in turn was perhaps linked to the increased salinity of the subtropical waters. In the case when Arctic freshwater was put directly into the East Greenland Current region, the SSS field (Figure 12a) did a fairly reasonable job of reproducing the climatological Levitus SSS field (Figure 12b) although it is clear that runoff from rivers such as

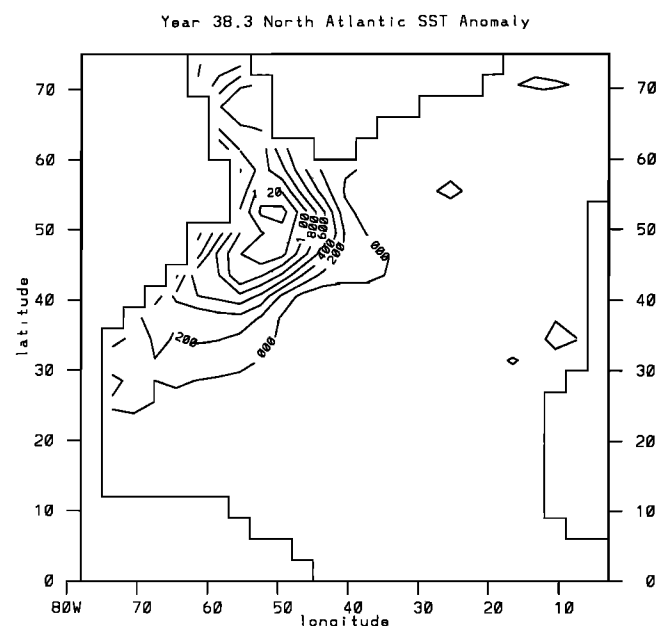


Figure 11c. Same as Figure 11a but corresponding to the strong phase.

the Amazon and the St. Lawrence, outflow from marginal seas such as the Mediterranean, and cross-equatorial water mass transport should be incorporated if one expects *Schmitt et al.*'s [1989] PE fields to drive a more realistic ocean climatology. Adding additional runoff sources would also weaken the parameterized equatorial freshwater flux (determined solely from the requirement of zero net salt input into the model domain) and hence increase the salinity in the subtropical waters. Notice also that the salinity maximum in the middle of the subtropical gyre is not as distinct as in reality.

The role of bottom topography on the stability and variability of the thermohaline circulation has also not been treated adequately. Most of the above uncoupled OGCM simulations assumed a flat ocean bottom. *Moore and Reason* [1993] suggest that some of the internal variability of the thermohaline circulation might be sensitive to the inclusion of bottom topography although it is not clear how well this topography is resolved in their 12-level model. In experiments T1–T3, bottom topography was incorporated into the model, the results of which are summarized in Table 1.

In experiment T1, full topography (which was manually digitized onto our 3° by 3° grid and smoothed using a 5-point filter) was used in the North Atlantic model. The smoothing used on this topography (continental shelf regions with deep ocean) had the effect of making the Labrador Sea less than 840 m deep everywhere. The net result was that the variability was suppressed. In experiment T2 the Labrador Sea region was dredged to be flat (4020 m deep), with full topography elsewhere in the domain. In this case the variability reappeared with the same timescale and dynamics as in experiments 4 and 5. In the final experiment, T3, the topography in the Labrador Sea region was left alone and the rest of the ocean (with the exception of continental shelf regions) was dredged to be 4020 m deep. The internal variability was once more suppressed.

The conclusions that one can draw from these experiments are limited. The Labrador Sea region is very poorly resolved (being only three tracer points wide) and hence the topography used was not representative of the region. Because of smoothing of the topography the Labrador Sea ended up being far too shallow and hence deep convection, strong east-west pressure gradients, and a fully developed thermohaline circulation could not occur. Much finer resolution horizontally should be used before a more complete understanding of the role of topography is obtained.

3.4. Relative Role of Thermal, Freshwater Flux and Wind Forcing

As discussed in section 3.2, the mechanism for the internal variability is very different from that found by *Weaver and Sarachik* [1991a, b] and *Weaver et al.* [1991]. To quantitatively show this, we conducted four more experiments in which we investigated the relative importance of thermal, freshwater flux, and wind forcing. In the first of these experiments (F1; Table 1) we started with an initial condition taken at year 3422 of experiment 1 and set the PE forcing to zero everywhere. The model was then integrated for a further 958 years, and to our surprise the variability remained largely unchanged with a period of 22 years. To test that our result was not somehow biased by the initial condition, we repeated experiment F1 except now we started from an initially resting, homogeneous ocean with 5°C temperature and 35.12 psu salinity everywhere (experi-

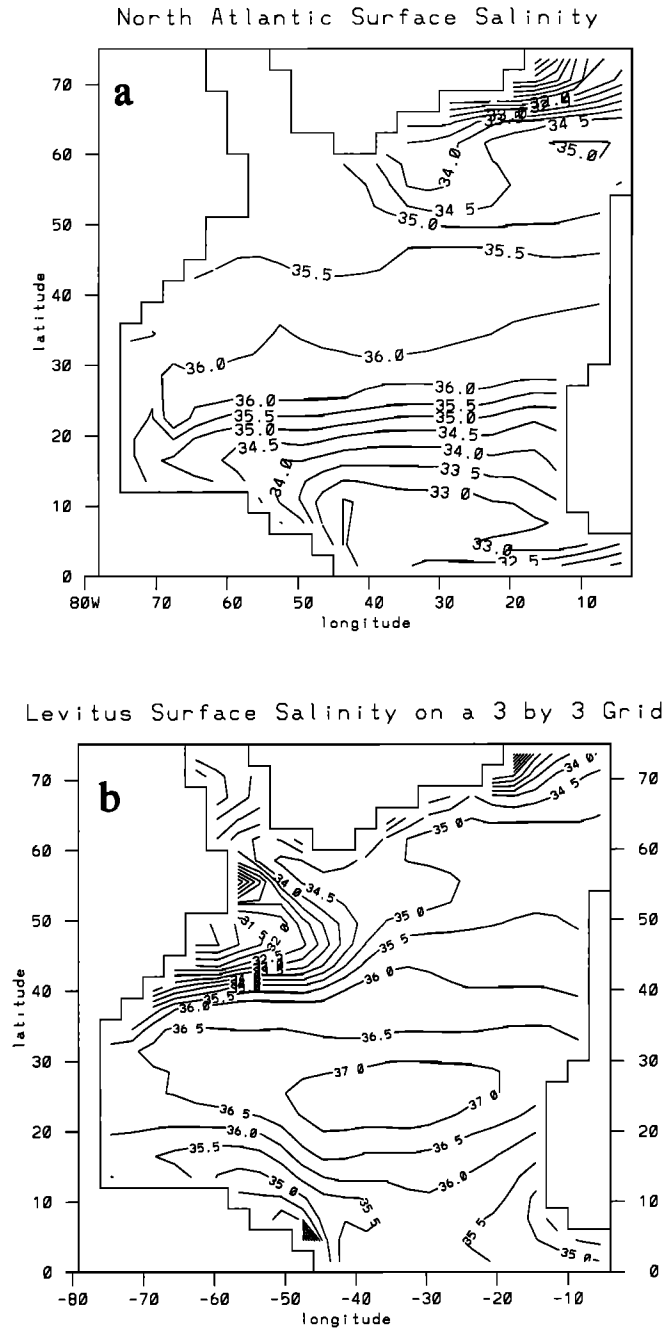


Figure 12. (a) A snapshot of the surface salinity field (in practical salinity units) from experiment 5. In this experiment 0.1 Sv freshwater was added only in the East Greenland Current region of the GIN Sea as a parameterization of Arctic freshwater export into the North Atlantic. Experiment 5 underwent internal variability with a period of about 17 years. (b) Levitus' [1982] sea surface salinity field (in practical salinity units) interpolated onto a 3° by 3° grid.

ment F2; Table 1). This model was integrated forward for 2738 years and once more the variability appeared with the same nature, timescale, and mechanism.

The next step was to investigate whether wind forcing was influencing our variability. In experiments F3 and F4 we repeated experiments F1 and F2 but now also set the wind forcing to zero everywhere (the model is now only thermally driven). The variability still occurred with the same nature,

timescale, and mechanism. Indeed, the magnitude of the basin-averaged heat flux over an oscillation was almost identical in experiments 1 and F1–F4.

To this point all the ocean-modeling studies that the authors are aware of required a “haline dominant” regime for the existence of internal variability of the thermohaline circulation. In this particular study we have demonstrated and documented a mechanism for interdecadal variability which can exist in a thermally dominant regime. We call this oscillation a thermally driven convective/advective oscillation.

4. Summary

In this paper we have discussed the mechanism and timescale of the thermohaline variability found in our coarse resolution simulations of the North Atlantic driven by observed forcing fields. We noted that the source for the variability was the Labrador Sea region of our model. In the slow phase of the oscillation, while the Labrador Sea was cooling, weak overturning occurred at the southwest boundary of Greenland. This deep-water formation region then moved to the northern wall of the Labrador Sea during the strong phase of the oscillation (once the cooling process/zonal overturning had set up a sufficiently strong zonal pressure gradient). The timescale of the variability was 22 years.

There are, of course, several fundamental interactions within the climate system that are missing from our model so one should view our results with caution. Our use of mixed boundary conditions implies an infinite heat capacity atmosphere which is clearly a crude approximation. Furthermore, there is no feedback of the SST on the hydrological cycle. Our model does not contain an ice component. As shown by *Yang and Neelin* [1993] and *Zhang et al.* [1994], ice/thermohaline interactions alone can provide mechanisms for thermohaline variability. It is also not clear whether or not the variability found in this coarse resolution model would carry over to a more realistic eddy resolving OGCM simulation. This is particularly worrying since the Labrador Sea was the most dynamically important region of the model yet the resolution in the Labrador Sea was very coarse.

In the coupled atmosphere-ocean simulations of *Delworth et al.* [1993] the thermohaline circulation of the North Atlantic Ocean was found to undergo variability on the 40–50 year timescale. The ocean surface characteristics of their model variability, as well as the location of its source, agree fairly well with the ocean only results conducted herein. It is not clear, however, to what extent the variability in the coupled ocean-atmosphere model is preconditioned by the mean PE field (flux correction plus annual mean). If the flux correction plus annual mean term is large in magnitude and of a form which contains much high-latitude structure, one might expect that the oceanic variability is determined by this structure with the higher-frequency PE variability providing a stochastic forcing which excites the variability (as in the earlier modeling studies of, for example, *Weaver et al.* [1991, 1993]). The high-latitude variability in the atmosphere and ice components of the climate system would then be forced by the internal thermohaline dynamics. Alternatively, it is plausible that a thermally-driven convective/advective mechanism might exist in *Delworth et al.*'s [1993] coupled atmosphere-ocean-ice model. If this is the case, the differ-

ence in the timescales between their 40–50 year oscillation and the present 22-year oscillation could be associated with a longer cooling time of their Labrador Sea and/or a slower overturning timescale. This in turn could be due to the replacement of the restoring boundary condition and “apparent atmosphere” in our model by a fully interactive prognostic atmosphere. One would also expect the fully coupled model to dampen the ocean only model variability.

R. Dickson (personal communication, 1992) suggested that the existence of shallow sills such as the Greenland-Iceland rise and the Iceland-Faroe rise may act to integrate out any variability in the GIN Seas so that overflow waters tend to be relatively time-invariant. This would be consistent with the *Dickson et al.* [1990] observation of the relatively constant water mass properties of the Denmark Strait Overflow waters between June 1987 and July 1989 and the OGCM simulation of *Moore and Reason* [1993]. On the other hand, no such sill exists across the Labrador Sea or its outflow regions. The western North Atlantic is also the region of the most dramatic changes found in the present ocean only study, the SST observations of *Kushnir* [1994], and the coupled ocean-atmosphere simulation of *Delworth et al.* [1993]. It is therefore tempting to speculate that much of the decadal/interdecadal variability observed in the Atlantic (e.g., *Levitus*, 1989a, b, c, 1990; *Kushnir*, 1994) is linked to changes in the water mass formation properties of the Labrador Sea. However, dramatic climatic events (e.g., Younger Dryas, etc.) may well be linked to the change in properties of the Denmark Strait overflow (or lack thereof).

Acknowledgments. AJW acknowledges support in the form of NSERC, NSERC/WOCE, AES, and DFO operating grants. We are grateful to J. Marotzke for providing us with Schmitt et al.'s (1989) PE fields and to two anonymous reviewers for their comments.

References

- Bjerknes, J., Atlantic air-sea interaction, *Adv. Geophys.*, *10*, 1–82, 1964.
- Bryan, K., and R. Stouffer, A note on Bjerknes' hypothesis for North Atlantic variability, *J. Mar. Syst.*, *1*, 229–241, 1991.
- Cattle, H., Diverting Soviet rivers: Some possible repercussions for the Arctic Ocean, *Polar Rec.*, *22*, 485–498, 1985.
- Cox, M. D., A primitive equation, three-dimensional model of the ocean, *Ocean Group Tech. Rep. 1*, Geophys. Fluid Dyn. Lab., Princeton, N. J., 1984.
- Delworth, T., S. Manabe, and R. J. Stouffer, Interdecadal variability of the thermohaline circulation in a coupled ocean-atmosphere model, *J. Clim.*, *6*, 1993–2011, 1993.
- Dickson, R. R., J. Meincke, S.-A. Malmberg, and A. J. Lee, The “Great Salinity Anomaly” in the northern North Atlantic 1968–1982, *Prog. Oceanogr.*, *20*, 103–151, 1988.
- Dickson, R. R., E. M. Gmitrowicz, and A. J. Watson, Deep-water renewal in the northern North Atlantic, *Nature*, *334*, 848–850, 1990.
- Ghil, M., and R. Vautard, Interdecadal oscillations and the warming trend in global temperature time series, *Nature*, *350*, 324–327, 1991.
- Gray, W. M., Strong association between West African rainfall and U.S. landfall of intense hurricanes, *Science*, *249*, 1251–1256, 1990.
- Greatbatch, R. J., A. F. Fanning, A. D. Goulding, and S. Levitus, A diagnosis of interpentadal circulation changes in the North Atlantic, *J. Geophys. Res.*, *96*, 22,009–22,023, 1991.
- Haney, R. L., Surface thermal boundary condition for ocean circulation models, *J. Phys. Oceanogr.*, *1*, 241–248, 1971.
- Hellerman, S., and M. Rosenstein, Normal monthly wind stress over the world ocean with error estimates, *J. Phys. Oceanogr.*, *13*, 1093–1104, 1983.

- Hibler, W. D., and S. J. Johnsen, The 20-year cycle in Greenland ice core records, *Nature*, **280**, 481–483, 1979.
- Ikeda, M., Decadal oscillations of the air-ice-ocean system in the northern hemisphere, *Atmos. Ocean*, **28**, 106–139, 1990.
- Krishnamurti, T. N., S.-H. Chu, and W. Iglesias, On the sea level pressure of the southern oscillation, *Arch. Meteorol. Geophys. Bioklimatol., Ser. A*, **34**, 385–425, 1986.
- Kushnir, Y., Interdecadal variations in North Atlantic sea surface temperature and associated atmospheric conditions, *J. Clim.*, **7**, 141–157, 1994.
- Lazier, J. R. N., Oceanographic conditions at Ocean Weather Ship BRAVO, 1944–1974, *Atmos. Ocean*, **18**, 227–238, 1980.
- Levitus, S., Climatological atlas of the World Ocean, *NOAA Prof. Pap. 13*, National Oceanic and Atmospheric Administration, Princeton, N. J., 1982.
- Levitus, S., Interpentadal variability of temperature and salinity at intermediate depths of the North Atlantic Ocean, 1970–1974 versus 1955–1959, *J. Geophys. Res.*, **94**, 6091–6131, 1989a.
- Levitus, S., Interpentadal variability of salinity in the upper 150 m of the North Atlantic Ocean, 1970–1974 versus 1955–1959, *J. Geophys. Res.*, **94**, 9679–9685, 1989b.
- Levitus, S., Interpentadal variability of temperature and salinity in the deep North Atlantic, 1970–1974 versus 1955–1959, *J. Geophys. Res.*, **94**, 16,125–16,131, 1989c.
- Levitus, S., Interpentadal variability of steric sea level and geopotential thickness of the North Atlantic Ocean, 1970–1974 versus 1955–1959, *J. Geophys. Res.*, **95**, 5233–5238, 1990.
- Loder, J. W., and C. Garrett, The 18.6-year cycle of sea surface temperature in shallow seas due to variations in tidal mixing, *J. Geophys. Res.*, **83**, 1967–1970, 1978.
- Moore, A. M., and C. J. C. Reason, The response of a global ocean general circulation model to climatological surface boundary conditions for temperature and salinity, *J. Phys. Oceanogr.*, **23**, 300–328, 1993.
- Myers, P. G., and A. J. Weaver, Low-frequency internal oceanic variability under seasonal forcing, *J. Geophys. Res.*, **97**, 9541–9563, 1992.
- Mysak, L. A., and D. K. Manak, Arctic sea-ice extent and anomalies, 1953–1984, *Atmos. Ocean*, **27**, 376–405, 1989.
- Mysak, L. A., D. K. Manak, and R. F. Marsden, Sea-ice anomalies in the Greenland and Labrador Seas during 1901–1984 and their relation to an interdecadal Arctic climate cycle, *Clim. Dyn.*, **5**, 111–133, 1990.
- Roemmich, D., and C. Wunsch, Apparent changes in the climatic state of the deep North Atlantic Ocean, *Nature*, **307**, 447–450, 1984.
- Schlosser, P., G. Bönisch, M. Rhein, and R. Bayer, Reduction of deepwater formation in the Greenland Sea during the 1980s: Evidence from tracer data, *Science*, **251**, 1054–1056, 1991.
- Schmitt, R. W., Bogden, P. S., and C. E. Dorman, Evaporation minus precipitation and density fluxes for the North Atlantic, *J. Phys. Oceanogr.*, **19**, 1208–1221, 1989.
- Weaver, A. J., and T. M. C. Hughes, Stability and variability of the thermohaline circulation and its link to climate, in *Trends in Physical Oceanography, Research Trends Ser.*, vol. 1, pp. 15–70, Council of Scientific Research Integration, Trivandrum, India, 1992.
- Weaver, A. J., and E. S. Sarachik, The role of mixed boundary conditions in numerical models of the ocean's climate, *J. Phys. Oceanogr.*, **21**, 1470–1493, 1991a.
- Weaver, A. J., and E. S. Sarachik, Evidence for decadal variability in an ocean general circulation model: An advective mechanism, *Atmos. Ocean*, **29**, 197–231, 1991b.
- Weaver, A. J., E. S. Sarachik, and J. Marotzke, Internal low frequency variability of the ocean's thermohaline circulation, *Nature*, **353**, 836–838, 1991.
- Weaver, A. J., J. Marotzke, P. F. Cummins, and E. S. Sarachik, Stability and variability of the thermohaline circulation, *J. Phys. Oceanogr.*, **22**, 39–60, 1993.
- Winton, M., and E. S. Sarachik, Thermohaline oscillations induced by strong steady salinity forcing of ocean general circulation models, *J. Phys. Oceanogr.*, **23**, 1389–1410, 1993.
- Yang, J., and J. D. Neelin, Sea ice interactions with the thermohaline circulation, *Geophys. Res. Lett.*, **20**, 217–220, 1993.
- Zhang, S., R. J. Greatbatch, and C. A. Lin, A reexamination of the polar halocline catastrophe and implications for coupled ocean-atmosphere modelling, *J. Phys. Oceanogr.*, **23**, 287–299, 1993.
- Zhang, S., C. A. Lin, and R. J. Greatbatch, A decadal oscillation in an ocean model coupled to a thermodynamic sea ice mode, *J. Mar. Res.*, in press, 1994.

S. M. Aura, Department of Atmospheric and Oceanic Sciences, McGill University, 805 Sherbrooke Street W., Montreal, Quebec, Canada H3A 2K6.

P. G. Myers and A. J. Weaver, School of Earth and Ocean Sciences, University of Victoria, P. O. Box 1700, Victoria, British Columbia, Canada V8W 2Y2.

(Received December 2, 1992; revised April 29, 1993; accepted June 25, 1993.)